American Mineralogist, Volume 89, pages 265–370, 2004

The structure of metahohmannite, $Fe_2^{3+}[O(SO_4)_2]\cdot 4H_2O$, by in situ synchrotron powder diffraction

FERNANDO SCORDARI,[1,*] GENNARO VENTRUTI,[1] AND ALESSANDRO F. GUALTIERI[2]

[1]Dipartimento Geomineralogico, Università di Bari I-70125 Bari, Italy
[2]Dipartimento di Scienze della Terra, Università di Modena e Reggio Emilia I-41100 Modena, Italy

ABSTRACT

Metahohmannite, $Fe_2^{3+}[O(SO_4)_2]\cdot 4H_2O$, is a hydrated sulfate of ferric iron that occurs in sulfate deposits in the desert areas of Northern Chile. The compound used for this study was obtained as a dehydration product of hohmannite, $Fe_2^{3+}[O(SO_4)_2]\cdot(4+4)H_2O$. Intensities for the structure analysis were collected from a powdered sample using in situ synchrotron X-ray powder diffraction at ESRF (Grenoble, France). The structure was solved ab initio by profile deconvolution and the application of standard Patterson and difference Fourier maps. The structure was refined to $R_p = 5.46\%$ using the Rietveld method. Metahohmannite crystallizes in the triclinic system, space group $P\bar{1}$ with unit-cell parameters $a = 7.3484(5)$ Å, $b = 9.7710(6)$ Å, $c = 7.1521(5)$ Å, $\alpha = 91.684(5)°$, $\beta = 98.523\ (5)°$, $\gamma = 86.390\ (5)°$, and $Z = 2$. The structure consists of four Fe^{3+} octahedra and four sulfate tetrahedra, which share vertices and edges to form a complex building block of $Fe_4^{3+}[O_2(SO_4)_4]\cdot 8H_2O$ composition. Such blocks are connected to form chains running parallel to the **c** axis. A complicated system of hydrogen bonds connects adjacent chains into a three-dimensional network. Finally, the crystal structures of metahohmannite, hohmannite, and amarantite are compared and the geometrical features discussed in detail.

INTRODUCTION

Metahohmannite was first described by Bandy (1938) as a hydrated sulfate of ferric iron associated with other secondary sulfates occurring in sulfate deposits in the desert areas of Northern Chile. According to Bandy (1938), metahohmannite is a member of the amarantite group, which is made up of three minerals with different water contents: hohmannite $Fe_2^{3+}[O(SO_4)_2]\cdot(4 + 4)H_2O$, amarantite $Fe_2^{3+}[O(SO_4)_2]\cdot(4 + 3)H_2O$, and metahohmannite $Fe^{3+}[O(SO_4)]\cdot 1.5H_2O$ (Bandy 1938; Strunz and Nickel 2001). Hohmannite appears to be the precursor of amarantite and is an unstable mineral, especially under dry conditions, where it readily transforms by successive dehydration steps into amarantite and then metahohmannite. Crystal structure determinations and/or accurate chemical analyses performed on hohmannite, amarantite, butlerite, and parabutlerite, $Fe^{3+}[OH(SO_4)]\cdot 2H_2O$, and fibroferrite, $Fe^{3+}[OH(SO_4)]\cdot 5H_2O$ (Fanfani et al. 1971; Borène 1970; Süsse 1968; Giacovazzo and Menchetti 1969; Scordari 1978, 1981) show that in amarantite and hohmannite the OH^- group substitutes for O^{2-}. Dehydration ↔ rehydration of hohmannite ↔ metahohmannite is easy and reversible, so the chemical formula proposed by Bandy (1938) for metahohmannite $[Fe_2(SO_4)_2(OH)_2\cdot 3H_2O]$ and halved in Strunz and Nickel (2001), seems to be unrealistic. The problem of the correct chemical formula is, to date, unsolved. Crystallographic data for metahohmannite are limited and poor. Apart from a short and unindexed powder pattern (Césbron 1964), no other structural data concerning this material are found in the literature. Because metahohmannite usually occurs in nature as loose, poorly coherent powdery masses, no single crystals are available for structure solution.

The development of X-ray powder diffraction profile-fitting methods combined with the use of high-intensity synchrotron sources allowing the collection of high-resolution powder diffraction patterns, makes it possible to achieve the ab initio structure determination of microcrystalline inorganic compounds. The present study is part of a systematic investigation of the phase transformations of hohmannite with temperature-induced dehydration using in situ time-resolved synchrotron powder diffraction. We report here the ab initio determination of the crystal structure of metahohmannite with a description of the basic structural features and the relationship with hohmannite and amarantite.

EXPERIMENTAL METHODS

The metahohmannite sample was obtained by heating a sample of hohmannite from Northern Chile, with the following crystal chemical formula: $Fe_2(H_2O)_4[(SO_4)_2O]\cdot 4H_2O$ (Scordari 1978). Intensities for the structure solution were collected during a synchrotron real-time powder diffraction experiment performed at the Italian beamline BM8 at ESFR (Grenoble, France). The BM8 beamline geometry is described in detail by Meneghini et al. (2001). The capillary (0.5 mm diameter) sample was mounted on a standard goniometer head. Data collection was done with parallel beam Debye geometry and a monochromatized fixed wavelength of 0.6888 Å calibrated with FIT2D (Hammersley 1998) against the NBS-640b Si standard with $a = 5.43094(4)$ Å at 298 K.

The temperature was raised using a heating gun system and monitored with a thermocouple positioned about 0.5 mm below the capillary. Temperature resolved experiments were performed by continuous heating of the hohmannite sample and the two-dimensional diffraction circles were recorded on an image plate (IP) detector (Amemija 1990) mounted perpendicular to the incoming beam at a distance of 257 mm. The IP detector is mounted on a translating system (TIPS: Norby 1996; Meneghini et al. 2001) behind a steel screen with a vertical 3 mm slit. The heating rate (5 °C/min) was synchronized with the speed of the translating system. The image stored in the IP was recovered using a Molecular Dynamics scanner with a dynamical range of 16 bit/pixel and a minimum pixel size of $50 \times 50\ \mu m^2$ (Fig. 1a). Slices of intensity representing a specified temperature range, encompassing about 11 K each, were extracted from the stored digitized file with a specially developed program SCANTIME developed for the extraction of powder patterns (see the three-dimensional 2θ-intensity-temperature diagram in Fig. 1b). The unit-cell

* E-mail: f.scordari@geomin.uniba.it

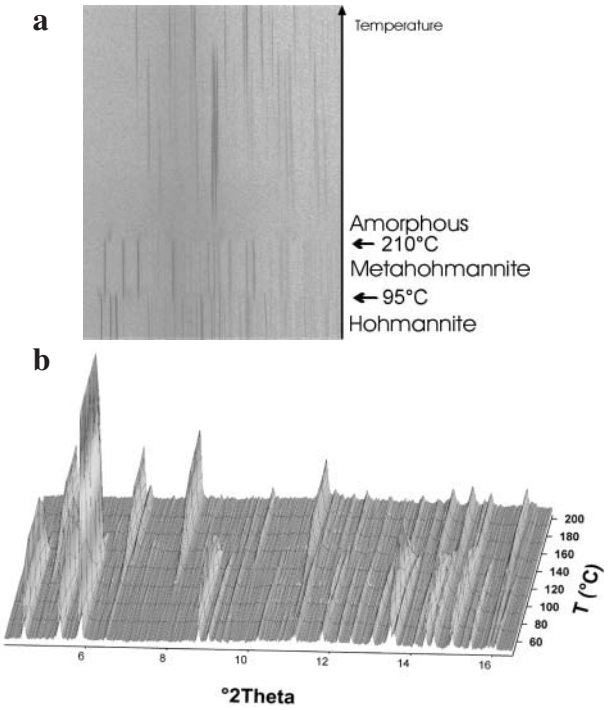

FIGURE 1. (**a**) The image obtained from the IP and (**b**) the three-dimensional plot (2θ-intensity-temperature) extracted by integration in the direction normal to the IP translation in which the 4–17 °2θ region is reported in the temperature range 60–200 °C.

dimensions were first determined by powder indexing using the program TREOR (Werner et al. 1985) and the indexing procedure indicated a triclinic cell. The cell parameters were refined by fitting the whole data set. Rietveld refinements were performed using the GSAS program package of Larson and Von Dreele (2000). Determination of the starting atomic coordinates was done with the aid of three-dimensional Patterson and Fourier syntheses in GSAS.

STRUCTURE SOLUTION AND REFINEMENT

In the first stage of the structure determination, the positions of 25 resolvable peaks of metahohmannite were accurately selected in the range 4–20 °2θ with an absolute error of 0.01 °2θ for each line. The peaks were all successfully indexed with a triclinic lattice with cell parameters a = 7.341(3) Å, b = 9.780(5) Å, c = 7.166(5) Å, α = 91.68(6)°, β = 98.45(3)°, γ = 86.35(5)°, and with the figures of merit (de Wolff 1968; Smith and Snyder 1979) M20 = 25 and F20 = 86 (0.004425, 53). The measured powder diffraction pattern at T = 154 °C was then fitted with the Le Bail method in GSAS. The powder pattern was subsequently refined in space group $P\bar{1}$, by analogy to hohmannite and amarantite. Only the lattice and profile parameters were used to describe the position and shape of all Bragg peaks, adjusting iteratively the intensity of the peaks. A pseudo-Voigt function was used to model the profile shape with a Gaussian coefficient GW and two Lorentzian coefficients LX and LY refined simultaneously. The 2θ zero shift was refined and only fixed points were used for modeling the background function.

Attempts to find an approximate structure model using direct methods failed (Altomare et al. 1999) but useful information was deduced from the Patterson synthesis and was applied to the powder diffraction data for the ab initio structure determination. The Patterson map showed the location of the heavy atoms (Fe,S). A Rietveld refinement was attempted using only the heavy atoms followed by difference-Fourier calculations. The remaining O atom positions were found, and a sound starting model containing all non-H atoms was obtained.

The structure was then successfully refined using GSAS. The sample heated at T = 154 °C shows a minor phase, $FeSO_4OH$ (Johansson 1962), which was included in the refinement. However another phase, possibly $Fe_2S_2O_9{\cdot}5H_2O$ (Levy and Quemeneur 1968), with peaks at 5.04, 4.47, 3.09, and 2.52 Å was present in the powder pattern. The diffraction peaks were again modeled with a pseudo-Voigt function with three Gaussian and two Lorentzian line-broadening coefficients. The background was fitted with a Chebyshev polynomial with 14 coefficients due to the incoherent contribution of the quartz capillary. Atomic coordinates and isotropic thermal parameters were refined in the later stages of the refinement. During refinement of the atomic positions, soft constraints were applied to the S-O and Fe-O distances to slowly converge toward a stable minimum, gradually reducing the weighting factor in the final cycles. Due to the impurity phases present in all patterns, the relatively short 2θ interval with observed intensities, and the severe line overlap that makes the estimation of the background more difficult, it was not possible to refine individual atomic displacement parameters. As a consequence, only an overall atomic displacement was refined for each atomic species. The refinement of the two phases quoted above converged to the following reliable indices: R_p = 6.15%, R_{wp} = 7.81, and $R(F^2)$ = 11.0%.

A better fit with R_p = 5.46% and R_{wp} = 6.94% was obtained for the pattern at 186 °C. At this temperature, the unknown phase disappears and the sample contains only two phases, metahohmannite and $FeSO_4OH$, with the second one predominant. The refinement was performed with the same criteria discussed above.

The atomic positions refined for the data sets collected at T = 154 °C and T = 186 °C were not significantly different. Hence, only the results at T = 186 °C (crystal data and atomic positions) were included in Table 1 and 2. For sake of comparison, the atom labels are equal to those reported by Scordari (1978). The final observed, calculated, and difference powder diffraction patterns resulting from the Rietveld refinement using the T = 186 °C data set are plotted in Figure 2. The observed and calculated patterns are available on request from the authors.

STRUCTURE DESCRIPTION AND DISCUSSION

The structure of metahohmannite projected along the **c** and **a** axes is shown in Figures 3a and 3b respectively. It is possible to recognize a cluster with $Fe_4(H_2O)_8O_2(SO_4)_4$ composition. The same Fe^{3+} cluster is also present in the structures of hohmannite and amarantite. Therefore, according to Bandy's (1938) nomenclature, metahohmannite represents the lower term of the series hohmannite-amarantite-metahohmannite, in which all the interstitial water molecules, not linked directly to cations, are lost. This assumption was also confirmed by means of the Platon program (Spek 1997). We checked for the presence of possible solvent accessible (H_2O) voids in metahohmannite structure; there were none.

The Fe^{3+} clusters polymerize via O8 to form chains of Fe-O-S

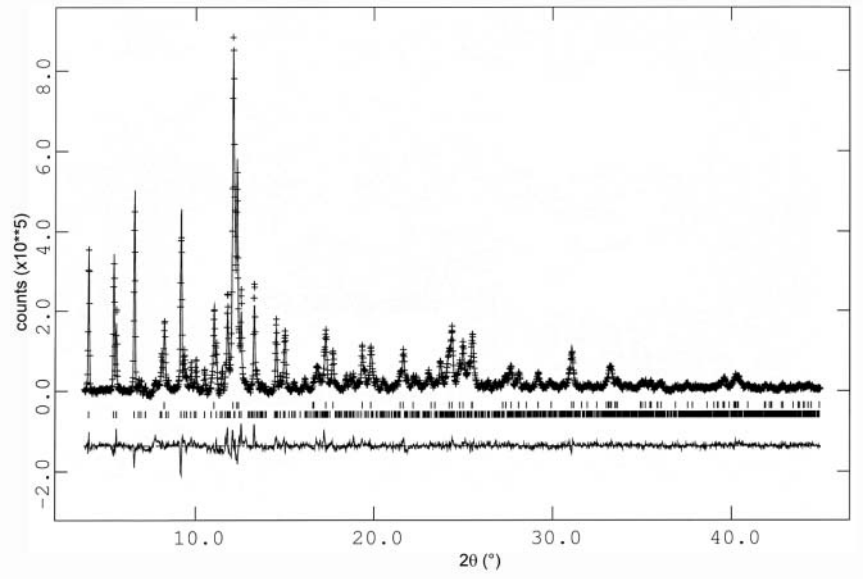

FIGURE 2. Final observed (crosses) and calculated (solid line) patterns for the Rietveld refinement at T = 186 °C. The difference pattern is shown below the Bragg markers.

TABLE 1. Crystal data and Rietveld refinement parameters for metahohmannite (T = 186 °C)

Formula sum	$Fe_4S_4O_{26}H_{16}$
Formula weight	783.76
Crystal system	triclinic
Space group	$P\bar{1}$
Unit-cell dimensions	a = 7.3484(5) Å
	b = 9.7710(6) Å
	c = 7.1521(5) Å
	α = 91.684(5)°
	β = 98.523(5)°
	γ = 86.390(5)°
Cell volume	506.74(6) Å^3
Density, calculated	2.568 g/cm^3

R_{wp} = 6.94 %
R_p = 5.46 %

Note: These were 4151 profile points. Reflection data statistics: no.observations (structure factors) = 1589 and R(F^2) =11.43%.

TABLE 2. Atomic coordinates and isotropic displacement parameters (in Å^2) for metahohmannite

Atom	Wyckoff	x	y	z	U_{iso}
Fe1	2*i*	0.622(1)	0.463(1)	0.356(2)	0.022(3)
Fe2	2*i*	0.636(1)	0.226(1)	0.709(1)	0.022(3)
S1	2*i*	0.885(2)	0.180(1)	0.374(2)	0.019(4)
S2	2*i*	0.349(2)	0.333(1)	0.000(2)	0.019(4)
O1	2*i*	0.816(3)	0.147(2)	0.548(3)	0.027(4)
O2	2*i*	1.085(2)	0.170(3)	0.412(4)	0.027(4)
O3	2*i*	0.163(3)	0.677(2)	0.682(4)	0.027(4)
O4	2*i*	0.787(4)	0.083(3)	0.246(3)	0.027(4)
O5	2*i*	0.309(3)	0.459(2)	0.890(3)	0.027(4)
O6	2*i*	0.503(3)	0.253(2)	0.938(3)	0.027(4)
O7	2*i*	0.185(3)	0.253(3)	-0.020(4)	0.027(4)
O8	2*i*	0.597(3)	0.631(3)	0.797(2)	0.027(4)
O9	2*i*	0.502(3)	0.631(2)	0.458(3)	0.027(4)
W11	2*i*	0.251(4)	0.957(2)	0.180(5)	0.027(4)
W12	2*i*	0.595(3)	0.871(3)	0.395(4)	0.027(4)
W14	2*i*	0.821(4)	0.558(3)	0.533(4)	0.027(4)
W16	2*i*	0.868(3)	0.320(3)	0.827(5)	0.027(4)

linkages along the **c** axis. The main features of this building block are (1) Two crystallographically equivalent Fe1 cations sharing an edge (O9-O$\bar{9}$) and two non-equivalent Fe^{3+} cations (Fe1 and Fe2) within distorted O atom octahedra, sharing one corner (O9). The two independent Fe^{3+} cations are surrounded by O atoms and water molecules, with different ratios of ligands: Fe1 coordinates five O atoms and one water molecule, whereas Fe2 coordinates three O atoms and three water molecules. The water molecules are indicated by W in Table 2. (2) Two symmetrically unrelated $(SO_4)^{2-}$ groups are linked to the Fe octahedra by corner-sharing: S2 shares three corners, O5, O6, and O8, with three distinct Fe octahedra, while S1 shares only two O atoms, O1 and O3, with two independent Fe octahedra. The remaining unshared tetrahedral O atoms of S1 and S2 are connected to neighboring chains by hydrogen bonds belonging to octahedral waters.

A center of symmetry doubles the Fe1-, Fe2- and S1-, S2-polyhedra leading to the Fe^{3+}- cluster mentioned above. From inspection of the geometrical data reported in Table 3 it is possible to compare the interatomic distances of metahohmannite, hohmannite, and amarantite. Metahohmannite exhibits a slightly

TABLE 3. Comparison of atomic distances (Å) in metahohmannite, hohmannite and amarantite

	Metahohmannite	Hohmannite	Amarantite
Fe1-O3	2.07(1)	2.032(4)	2.042(6)
Fe1-O5	2.08(1)	2.045(4)	2.085(6)
Fe1-O8	2.05(1)	2.034(4)	2.045(6)
Fe1-O9	1.99(1)	1.949(4)	1.923(6)
Fe1-O$\bar{9}$	2.00(1)	1.935(4)	1.969(6)
Fe1-W14	2.04(1)	2.056(5)	2.091(6)
<Fe1-O>	2.04	2.009	2.026
Fe2-O1	1.99(1)	1.967(4)	1.986(6)
Fe2-O6	2.03(1)	1.996(4)	2.028(6)
Fe2-O9	1.99(1)	1.870(4)	1.892(6)
Fe2-W11	2.05(1)	2.100(5)	2.074(6)
Fe2-W12	2.02(1)	2.025(5)	2.052(6)
Fe2-W16	2.05(1)	2.066(5)	2.069(6)
<Fe2-O>	2.02	2.004	2.017
S1-O1	1.47(1)	1.481(5)	1.496(6)
S1-O2	1.46(1)	1.436(5)	1.456(6)
S1-O3	1.47(1)	1.483(4)	1.495(6)
S1-O4	1.45(1)	1.469(5)	1.456(6)
<S1-O>	1.46	1.467	1.476
S2-O5	1.47(1)	1.470(5)	1.489(6)
S2-O6	1.45(1)	1.466(4)	1.495(6)
S2-O7	1.46(1)	1.433(5)	1.439(6)
S2-O8	1.49(1)	1.473(4)	1.489(6)
<S2-O>	1.47	1.460	1.478

less distorted $(SO_4)^{2-}$ tetrahedra (Δ_{max} = 0.02 Å) with respect to the equivalent ones observed in hohmannite (Δ_{max} = 0.04 Å) and amarantite (Δ_{max} = 0.04 Å). However, the average S-O distances in metahohmannite are similar to the corresponding distances in hohmannite and amarantite within standard deviation. The effect of deformation is more marked for the Fe-octahedra because of differences concerning the hydrogen bond system; for instance, in metahohmannite H6 (see Table 4) points toward O9, extending Fe–O9 lengths. As a consequence the range of Fe–O bond distances in metahohmannite (Δ_{max} = 0.08 Å) is smaller than in hohmannite (Δ_{max} = 0.18 Å) and amarantite (Δ_{max} = 0.18 Å), whereas the mean lengths are about the same within two standard deviations. On the whole the main geometrical features of the polyhedra belonging to the Fe^{3+} cluster are preserved in the structure of metahohmannite. For example, the shortening of the Fe-O distances involving O9 and its equivalent $O\bar{9}$, and consequently the lengthening of the distance of the Fe1 cation from the two opposite O5 and O3 atoms is a common feature of all the quoted structures. The shortening of Fe-O9 distance is due to the position of O9 in the structure, almost at the center of the Fe1-Fe$\bar{1}$-Fe2 triangle. From a crystal-chemical standpoint the ideal bond strength reaching O9 is too low (1.5 v.u.), therefore the Fe^{3+}-O distances are shorter to fill the electrostatic gap involving the O9 atom. The shortening of Fe-O9 distances decrease slightly and the bond strength involving O9 improves (see Tables 3 and 4), if the contribution of H6 is taken into account. Similar arguments can be made to explain the splitting observed in the $(SO_4)^{2-}$ tetrahedral distances. The shorter distances, S1-O2 and S1-O4, are related to the two unshared O atoms of this group (see Table 3). As far as the S2 group is concerned, O7 is the only unshared tetrahedral O atom. Surprisingly, S2-O7 is not the shortest distance, as hohmannite and amarantite show. Results from two different techniques (single-crystal and powder) are compared here and it is known that single crystal results are more precise than those from the powder method. This can explain the less marked differences concerning the S2-O distances (see Table 3).

Fe^{3+} clusters polymerize via O8 to form chains of Fe-O-S linkages along **c**. The connection among these chains takes place throughout a complex system of hydrogen bonds. The diffusion of the interstitial waters during the dehydration process forces these clusters to change their configuration to adapt to the newly formed structure of metahohmannite. Accordingly, a rotation of the polymerized Fe^{3+} clusters, by about 20° with respect to hohmannite and about 40° with respect to amarantite has been measured (Fig. 4a). Moreover, changes of orientation of $(S1O_4)^{2-}$ tetrahedron are also observed. This group is free to rotate around the O1-O3 edge, and assumes different orientations in amarantite, hohmannite, and metahohmannite. The orientation angle has been measured between the planes determined by the Fe1-Fe2-Fe$\bar{1}$ and O1-S1-O2 atomic positions respectively. The values observed are about 175°, 170°, and 110° in hohmannite, amarantite, and metahohmannite, respectively (Fig. 4b). The re-

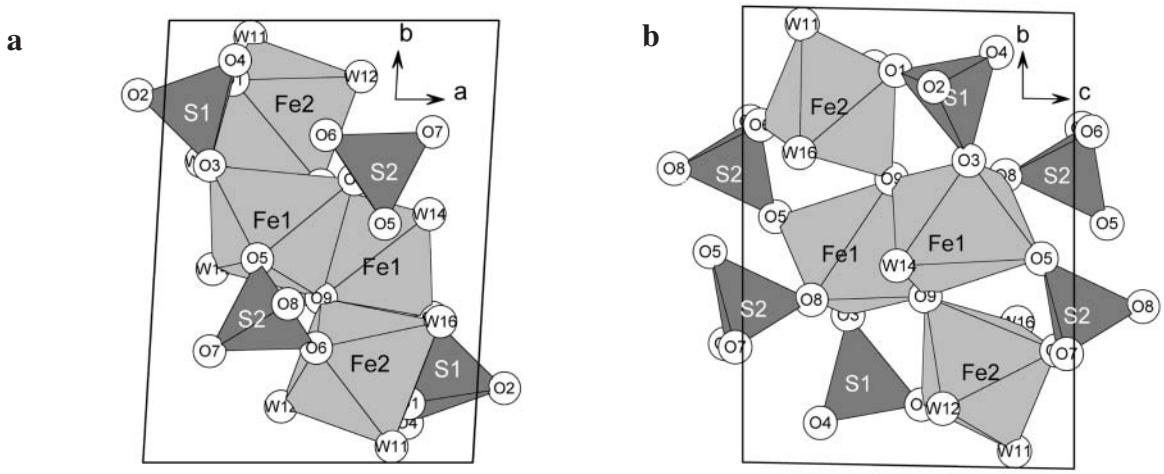

FIGURE 3. The crystal structure of metahohmannite projected along the **c** (**a**) and **a** axes (**b**).

TABLE 4. Bond valences and their sums (v.u.) for metahohmannite

	O1	O2	O3	O4	O5	O6	O7	O8	O9	W11	W12	W14	W16	S
Fe1			0.43		0.42			0.46	1.06			0.47		2.84
Fe2	0.54					0.48			0.54	0.46	0.49		0.46	2.97
S1	1.52	1.56	1.52	1.60										6.20
S2					1.52	1.60	1.56	1.44						6.12
H1							0.08			0.92				1.00
H2				0.12						0.88				1.00
H3				0.16							0.84			1.00
H4		0.29									0.71			1.00
H5		0.19										0.81		1.00
H6									0.37			0.63		1.00
H7					0.08								0.92	1.00
H8							0.33						0.67	1.00
Σincl.H	2.06	1.56	1.95	1.60	1.94	2.08	1.56	1.90	1.60	0.46	0.49	0.47	0.46	1.00
Σexcl.H	2.06	2.04	1.95	1.88	2.02	2.08	1.97	1.90	1.97	2.26	2.04	1.91	2.05	1.00

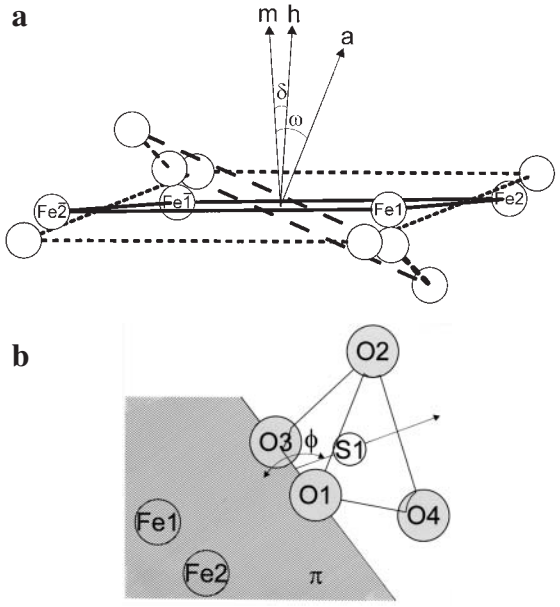

FIGURE 4. (**a**) Sketch of three Fe1-Fe2-Fe$\bar{1}$-Fe$\bar{2}$ planes in metahohmannite (full lines), hohmannite (broken lines), and amarantite (dotted lines). The normals to these planes are indicated with m, h, and a respectively. The angles between them, δ (~20°) and ω (~40°), represent the rotation the iron planes undergo during the phase transformation. (**b**) The rotation angle φ between S1 tetrahedra and the Fe1-Fe2-O1-O3 plane, calculated for the three phases (the values are given in the text).

TABLE 5. Distances (Å) between water molecules W11, W12, W14, and W16 and the closest proton acceptor O atom

W11		W12		W14		W16	
O2	2.94(4)^{v}	O2	2.56(3)^{vi}	O2	2.79(4)^{vi}	O5	3.26(4)^{vii}
O4	3.03(4)^{iii}	O4	2.90(4)^{iv}	O5	3.04(4)^{ii}	O7	2.48(3)^{viii}
O7	3.24(3)^{ix}	O9	2.55(3)^{i}	O9	2.39(3)^{i}	O9	3.17(3)^{ii}
				O9	3.11(4)^{ii}		

Notes: Symmetry codes: (i) *x*, *y*, *z*; (ii) 1 – *x*, 1 – *y*, 1 – *z*; (iii) 1 – *x*, 1 – *y*, –*z*; (iv) *x*, 1 + *y*, *z*; (v) –1 + *x*, 1 + *y*, *z*; (vi) 2 – *x*, 1 – *y*, 1 – *z*; (vii) 1 – *x*, 1 – *y*, 2 – *z*; (viii) 1 + *x*, *y*, 1 + *z*; (ix) *x*, –1 + *y*, *z*.

TABLE 6. Comparison between bond valence sums excluding H atoms of metahohmannite, hohmannite, and amarantite

	metahohmannite	hohmannite	amarantite
Fe1	2.84	3.083	2.958
Fe2	2.97	3.159	3.017
S1	6.20	6.118	5.980
S2	6.12	6.229	5.946
O1	2.06	2.042	1.954
O2	1.56*	1.662*	1.575*
O3	1.95	1.942*	1.882*
O4	1.60*	1.520*	1.575*
O5	1.94*	1.978	1.854*
O6	2.08	2.060	1.900
O7	1.56*	1.676*	1.649*
O8	1.90	1.980	1.902
O9	1.60*	1.960	1.907
W11	0.46	0.398	0.427
W12	0.49	0.487	0.453
W14	0.47	0.448	0.408
W16	0.46	0.436	0.433

* Indicates O atoms involved in the hydrogen bond system.

orientations of Fe-clusters just discussed cause disruption of the hydrogen-bond system of the old structure and the building of a more suitable system for the new structure. This system of bonds could not be resolved directly by difference-Fourier synthesis. A possible hydrogen bond scheme was proposed by cross-checking the results from electrostatic bond valence requirements and geometric considerations (Table 5).

The data of Breese and O'Keeffe (1991) were used to calculate the bond valences of all the non-H atoms, while the strengths of the O-H···O bonds were derived from the curve published by Brown and Altermatt (1985). The results indicate a remarkably low bond-valence sum for the O9 atoms in metahohmannite with respect to hohmannite and amarantite (Table 6). Therefore the O9 atoms must be regarded as proton acceptors, as discussed above. The hydrogen bond system proposed in Table 4 and deduced from the interatomic distances between water molecules and their closest O atom neighbors (Table 5) appears to be the best possible for the metahohmannite structure (Fig. 5). The loss of interstitial water molecules significantly influences some cell parameters in metahohmannite compared to hohmannite. In fact while *c*, which depends on the length of the Fe^{3+} cluster, is nearly unchanged ($c \approx 7.17$ Å), *b* and *a*, more directly involved in the water loss, are strongly influenced. The result of the structure analysis gives a structural interpretation to the thermal effects observed by Césbron (1964). In fact, thermal analyses performed by Césbron (1964) on crystals of hohmannite obtained by rehydration of amarantite show that in the range 95–143 °C the thermogravimetric analysis (TGA) curve of hohmannite displays a plateau similar to that of amarantite. This plateau has been attributed to the loss of three water molecules expelled from the hohmannite structure. From the dehydration of hohmannite a new compound arises having the same chemical formula proposed by Bandy (1938) for metahohmannite. The effects of water loss on the crystal structure and the building of the metahohmannite phase have been monitored here using in situ synchrotron powder diffraction. The collected data show that the structure of hohmannite is not greatly affected by the thermal treatment up to 66 °C, the diffraction patterns being virtually identical in peak position and intensity. The intensities of the hohmannite reflections decrease significantly in the range 80–100 °C. In agreement with the thermal analysis data discussed by Césbron (1964), the hohmannite structure is largely destroyed in the range 100–120 °C. Metahohmannite grows at 80 °C, increases in volume in the range 80–100 °C, and becomes the predominant phase at $T \geq 110$ °C. The appearance of metahohmannite around 80 °C is consistent with the TGA curve given by Césbron (1964), which records an abrupt weight loss that is completed at about 95 °C. Therefore the material heated above 110 °C contains metahohmannite with lesser amounts of impurity phases, of which only one, $FeSO_4OH$, was identified and refined. The decomposition of metahohmannite started at about 190 °C and is complete at 220 °C.

The structure of metahohmannite investigated here shows that: (1) metahohmannite is the last phase that can preserve the Fe^{3+} cluster present in hohmannite, and (2) other phases, like amarantite, with an interstitial water content ranging from three to zero water molecules, are possible.

In spite of the high number of powder diffraction lines arising from the low crystal symmetry and the presence of impurity phases, the crystal structure model proposed for metahohmannite appears to be satisfactory although some details of individual

interatomic distances and angles seem to be less reliable. Notwithstanding, the quality of the final agreement factors and the good fit of the Rietveld refinement are a proof of the reliability of the structure model derived herein from the Patterson method using powder diffraction intensities.

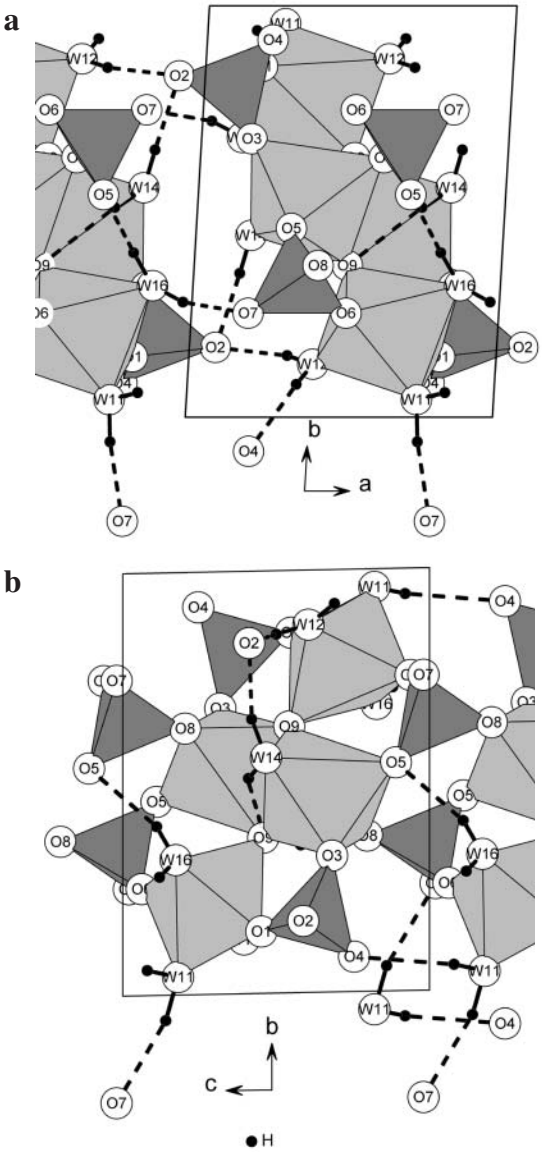

FIGURE 5. Proposed hydrogen-bond system in metahohmannite. To show all the hydrogen bonds, the structure of metahohmannite is projected along both the **c** (**a**) and **a** (**b**) axes.

ACKNOWLEDGMENTS

C. Meneghini of the GILDA staff is kindly acknowledged for help during the in situ experiment. C. Dalconi and G. Cruciani are also acknowledged for help during the data reduction and useful discussions.

REFERENCES CITED

Altomare, A., Burla, M.C., Camalli, M., Carrozzini, B., Cascarano, G., Giacovazzo, C., Guagliardi, A., Moliterni, A.G.G., Polidori, G., and Rizzi, R. (1999) EXPO: a program for full powder pattern decomposition and crystal structure solution. Journal of Applied Crystallography, 32, 339–340.

Amemija, Y. (1990) Imaging plate—X-ray area detector based on photostimulable phosphor. Synchrotron Radiation News, 3, 21–26.

Bandy, M.C. (1938) Mineralogy of three sulphate deposits of Northern Chile. American Mineralogist, 23, 669–760.

Borène, J. (1970) Structure cristalline de la parabutlerite. Bulletin Societe Francais de Mineralogie et Crystallographie, 93, 185–189.

Breese, N.E. and O'Keeffe, M. (1991) Bond-valence parameters for solids. Acta Crystallographica, B47, 192–197.

Brown, I.D. and Altermatt, D. (1985) Bond valence parameters obtained from a systematic analysis of the inorganic crystal structure database. Acta Crystallographica, B41, 244–247.

Césbron, F. (1964) Contribution à la Minéralogie des sulfates de fer hydratés Bulletin Societe Francais de Mineralogie et Crystallographie, 87, 125–143.

de Wolff, P.M. (1968) A simplified criterion for the reliability of a powder pattern indexing. Journal of Applied Crystallography, 1, 108–113.

Fanfani, L., Nunzi, A., and Zanazzi, P.F. (1971) The crystal structure of butlerite. American Mineralogist, 56, 751–757.

Giacovazzo, C. and Menchetti, S. (1969) Sulla struttura della amarantite. Rendiconti Società Italiana di mineralogia e petrologia, 25, 399–406.

Hammersley, A.P. (1998) FIT2D V10.3 Reference Manual V4.0 ESRF98HA01T.

Johansson, G. (1962) On the crystal structure of $FeOHSO_4$ and $InOHSO_4$. Acta Chemica Scandinavica, 16, 1234–1244.

Larson, A.C. and Von Dreele, R.B. (2000) General Structure Analysis System (GSAS). Los Alamos National Laboratory Report LAUR 86–748.

Levy, W.L. and Quemeneur, E. (1968) Sur la thermolyse des sulfates ferriques basiques. Bulletin De La Société Chimique De France, 2, 495–503.

Meneghini, C., Artioli, G., Balerna, A., Gualtieri, A.F., Norby, P., and Mobilio, S. (2001) Multipurpose imaging-plate camera for in-situ powder XRD at the GILDA beamline. Journal of Synchrotron Radiation, 8, 1162–1166.

Norby, P. (1996) In situ time-resolved synchrotron powder diffraction studies of syntheses and chemical reactions. Materials Science Forum, 147, 228–231.

Scordari, F. (1978) The crystal structure of hohmannite, $Fe_2(H_2O)_4[(SO_4)_2O]\cdot 4H_2O$ and its relationship to amarantite, $Fe_2(H_2O)_4[(SO_4)_2O]\cdot 3H_2O$. Mineralogical Magazine, 42, 144–146.

——— (1981) Fibroferrite: A mineral with a $\{Fe(OH)(H_2O)SO_4\}$ spiral chain and its relationship to $Fe(OH)SO_4$, butlerite and parabutlerite. Tschermaks Mineralogische und Petrographische Mitteilungen, 28, 17–29.

Smith, G.S. and Snyder, R.L. (1979) Fn: a criterion for rating powder diffraction patterns and evaluating the reliability of powder-pattern indexing. Journal of Applied Crystallography, 12, 60–65.

Spek, A.L. (1997) PLATON. Molecular Geometry Program. University of Utrecht. The Netherlands.

Strunz, H. and Nickel, E.H. (2001) Strunz Mineralogical Tables. Chemical Structural Mineral Classification System 9th edition, 870 S., 226 Abb., Best.-Nr. 13-3509.

Süsse, P. (1968) The crystal structure of amarantite, $Fe_2(SO_4)_2O\cdot 7H_2O$. Zeitschrift für Kristallographie, 127, 261–275.

Werner, P.E., Eriksson, L., and Westdahl, M. (1985) TREOR, a semi exhaustive trial-and-error powder indexing program for all symmetries. Journal of Applied Crystallography, 18, 367–370.

MANUSCRIPT RECEIVED MAY 23, 2003
MANUSCRIPT ACCEPTED AUGUST 19, 2003
MANUSCRIPT HANDLED BY BRYAN CHAKOUMAKOS